Supplementary Information

Enhanced Localized Surface Plasmon Resonance of fully alloyed AgAuPdPt, AgAuPt, AuPt, AgPt and Pt Nanocrystals: Systematical Investigation on the Morphological and LSPR Properties of Mono-, Bi-, Tri-, Quad-metallic Nanoparticles

Sundar Kunwar, Puran Pandey and Jihoon Lee*

Department of Electronic Engineering, College of Electronics and Information, Kwangwoon University, Nowon-gu Seoul 01897, South Korea

EXPERIMENTAL SECTION in more detail

In order to fabricate various multi-metallic alloy NPs, three different deposition schemes were adapted. In the 1st series, the 7.5 nm of Ag and 3.75 nm of Pt films were deposited in a sequence named as $Ag_{7.5nm}/Pt_{3.75nm}$ bilayer. Similarly, in the 2nd and 3rd sets, $Ag_{55nm}/Au_{15nm}/Pt_{15nm}$ tri-layers and $Ag_{40nm}/Au_{15nm}/Pd_{15nm}/Pt_{15nm}$ quad-layers were deposited respectively to fabricate the tri-metallic and quad-metallic alloy NPs. The deposition of all metal films was performed in a sputtering chamber under 1×10^{-1} Torr with 3 mA ionizations current at the growth rate of 0.05 nm/s.

For the characterization of surface nanostructures, atomic force microscope (AFM, XE-70, Parks System, South Korea) under a non-contact mode was adapted. The AFM scanning was performed with the same batch of tips to minimize tip effects. In addition, scanning electron microscope (SEM, CX-200, COXEM, South Korea) was employed for the large-scale morphological analysis. The elemental analysis of the various multi-metallic alloy NPs was carried out by using an energy dispersive x-ray spectroscope (EDS, Thermo Fisher Noran System 7). The optical spectra of these multi-metallic nanostructures were acquired by using an SR-500 spectrograph equipped with the CCD detector, optical microscope and light sources. For the excitation of samples, the combined deuterium and halogen light source were used, which covers the UV-VIS-NIR range of the electromagnetic spectrum. The reflectance and transmittance spectra were experimentally measured, and the extinction spectra were calculated by the relation, extinction (%) = 100 % - (reflectance + transmittance) %.

To investigate the e-field distribution of alloy NPs on sapphire, the simulations were performed using finite difference time domain (FDTD) solutions (Lumerical, Canada). The model was created using the imported AFM images, which was placed on a thick sapphire substrate. With the perfectly match layer boundary conditions in the x, y and z directions, the TFSF source polarized along the x-axis was utilized to excite the alloy NPs from the z-direction. The simulation time was 1000 fs with the sufficiently small mesh between 0.5 and 5 nm depending upon the size of NPs. The dielectric

constants of Au, Pd and Pt were referred from the Palik models and the Rakic constant was used for Ag. The dielectric constants of multi-metallic alloy NPs were averaged from the dielectric constant of the pure element based on the at. % fraction. For example, based on the ellipsometry measurement for a binary material, i.e. Ag-Pt, the dielectric constant varies along with the averaged value of at. % fraction. Thus, the Au-Pt dielectric constant was constructed by averaging based on the at. % fraction. Then, the dielectric constant for AuPtPd was again averaged based on the at. % fraction.

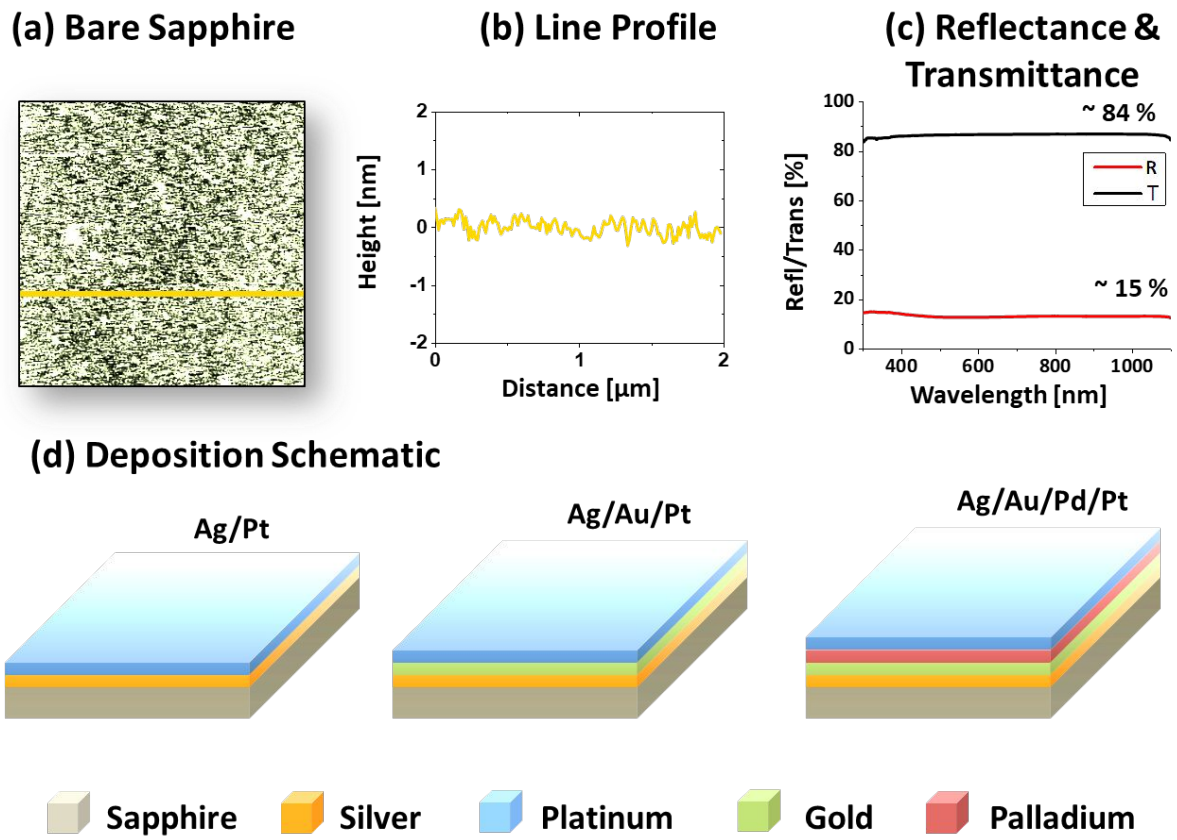

Figure S1: (a) Atomic force microscope (AFM) image of the bare sapphire (0001). (b) Cross-sectional line profile across the AFM image. (c) UV-vis-NIR reflectance and transmittance spectra of bare sapphire (0001). (d) Deposition schematics of Ag/Pt bilayer, Ag/Au/Pt trilayer and Ag/Au/Pd/Pt quad-layer as labeled.

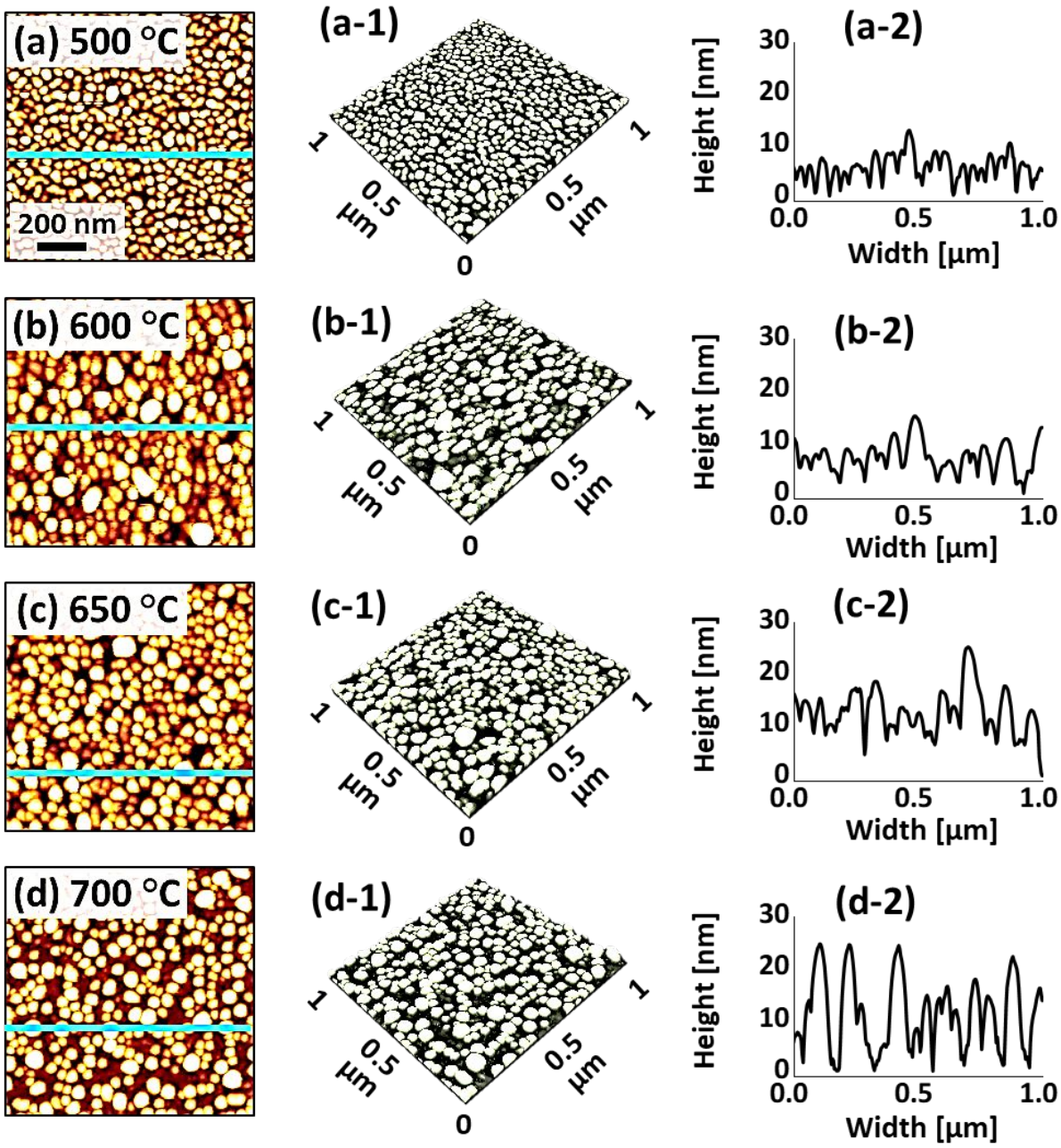

Figure S2: Formation of small and dense AgPt and Pt NPs from $Ag_{7.5nm}/Pt_{3.75nm}$ multilayer film by annealing between 500 and 700 °C. (a) – (d) AFM top-views of 1 × 1 µm^2. (a-1) – (d-1) Corresponding AFM side-views. (a-2) – (d-2) Cross-sectional line profiles.

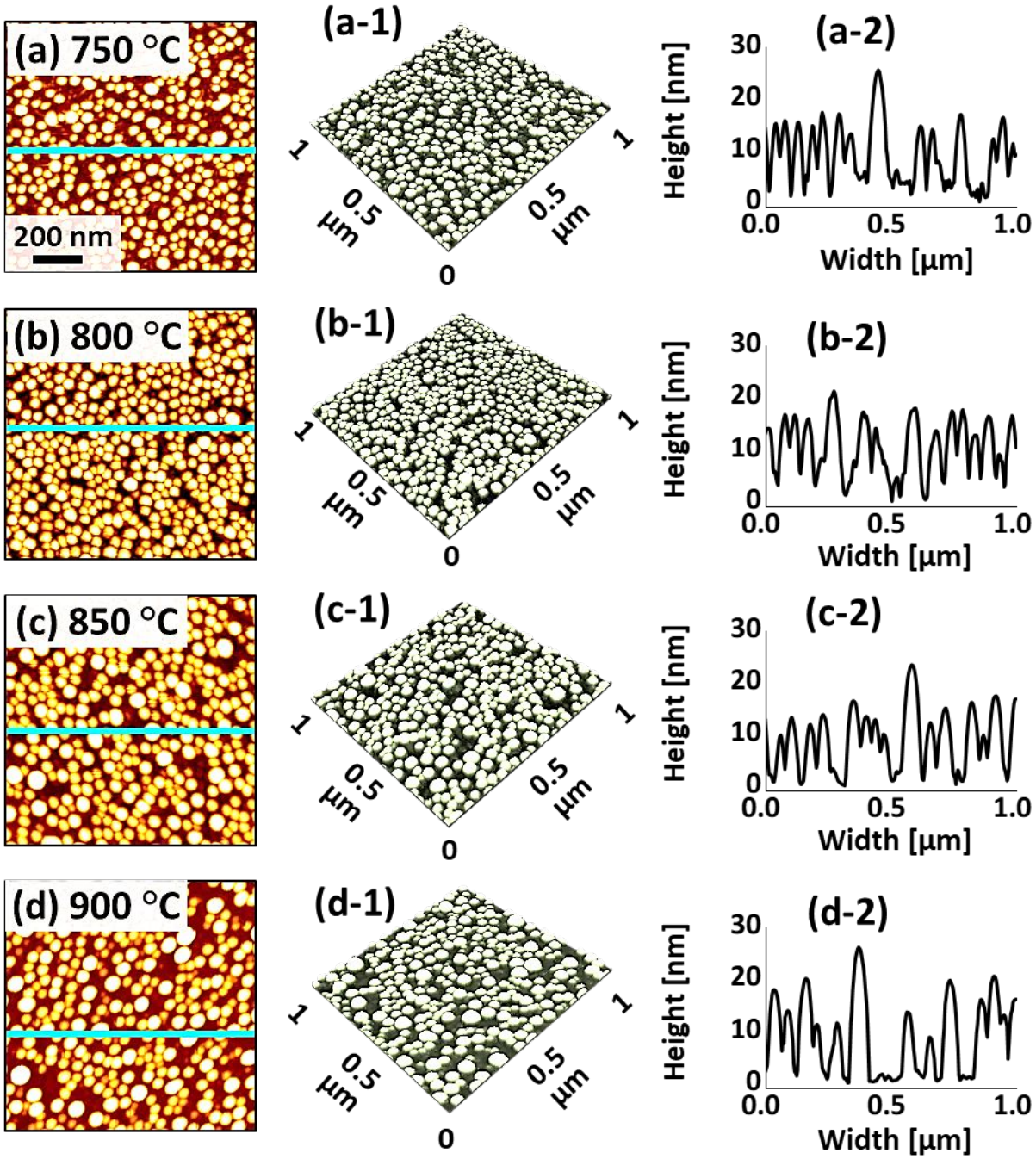

Figure S3: Evolution of Pt NPs by the annealing of $Ag_{7.5nm}/Pt_{3.75nm}$ bilayers film between 750 and 900 °C. (a) – (d) AFM top-views of 1 × 1 µm^2. (a-1) – (d-1) Corresponding AFM side-views. (a-2) – (d-2) Cross-sectional line profiles.

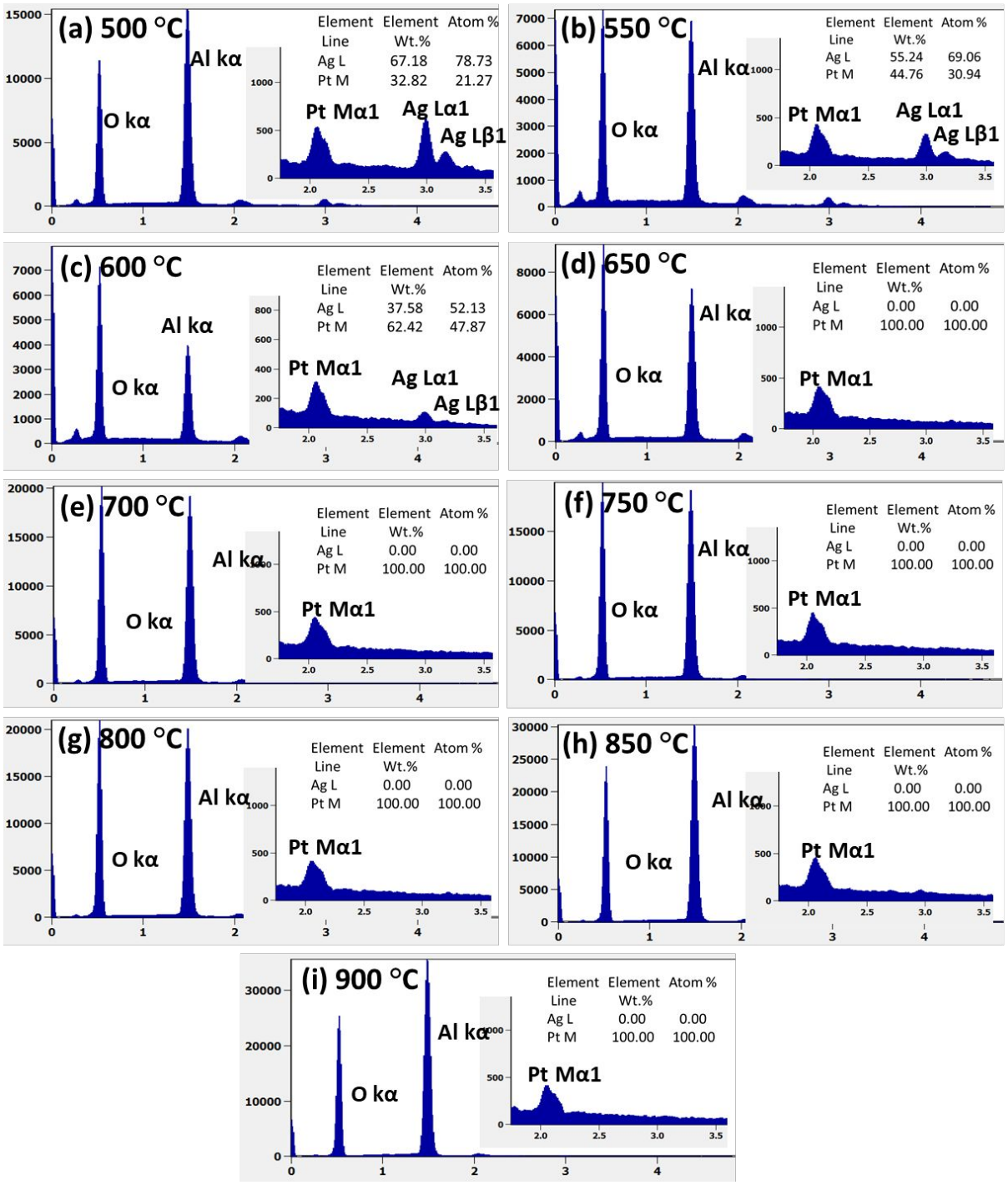

Figure S4: (a) – (i) EDS spectra of the samples fabricated with AgPt alloy NPs from $Ag_{7.5nm}/Pt_{3.75nm}$ bilayer by annealing between 500 and 900 °C for 120 s. Corresponding insets show the enlarged Pt and Ag peaks and elemental compositions in terms of atomic (at) % and weight (wt) %.

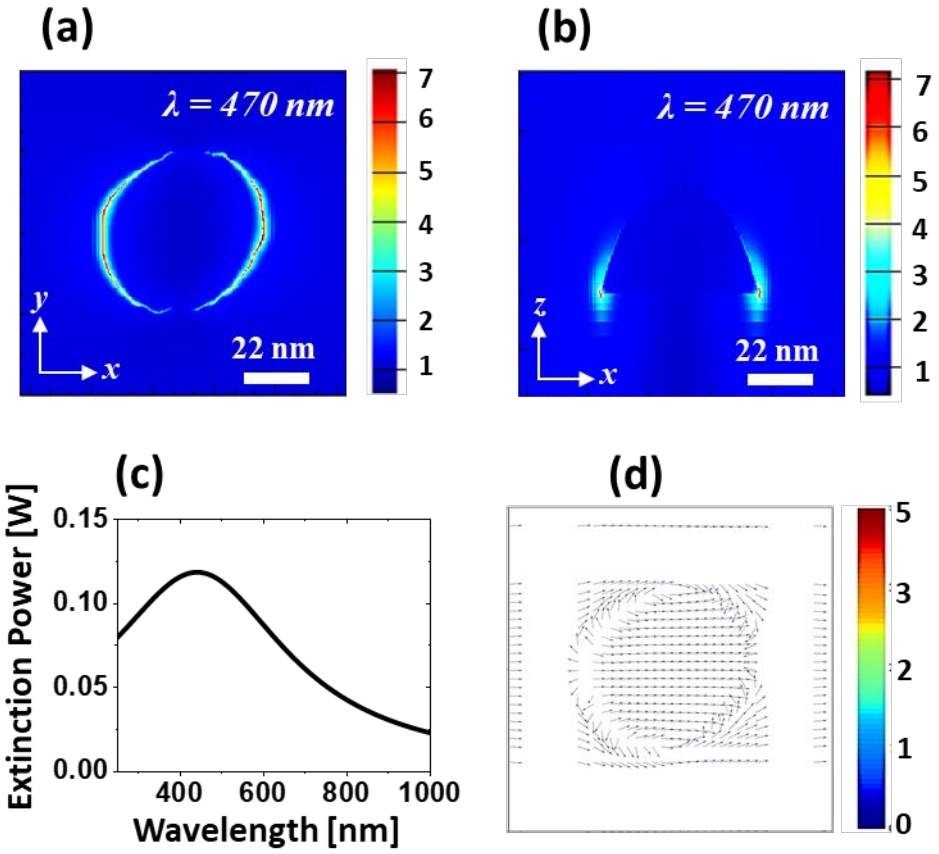

Figure S5: Finite difference time domain (FDTD) simulation of the small size Pt NP fabricated with the $Ag_{7.5nm}/Pt_{3.75nm}$ bilayer at 900 °C. (a) – (b) Top and side-view of the simulated e-field profiles. (c) Simulated extinction spectra. (d) E-field vector plot.

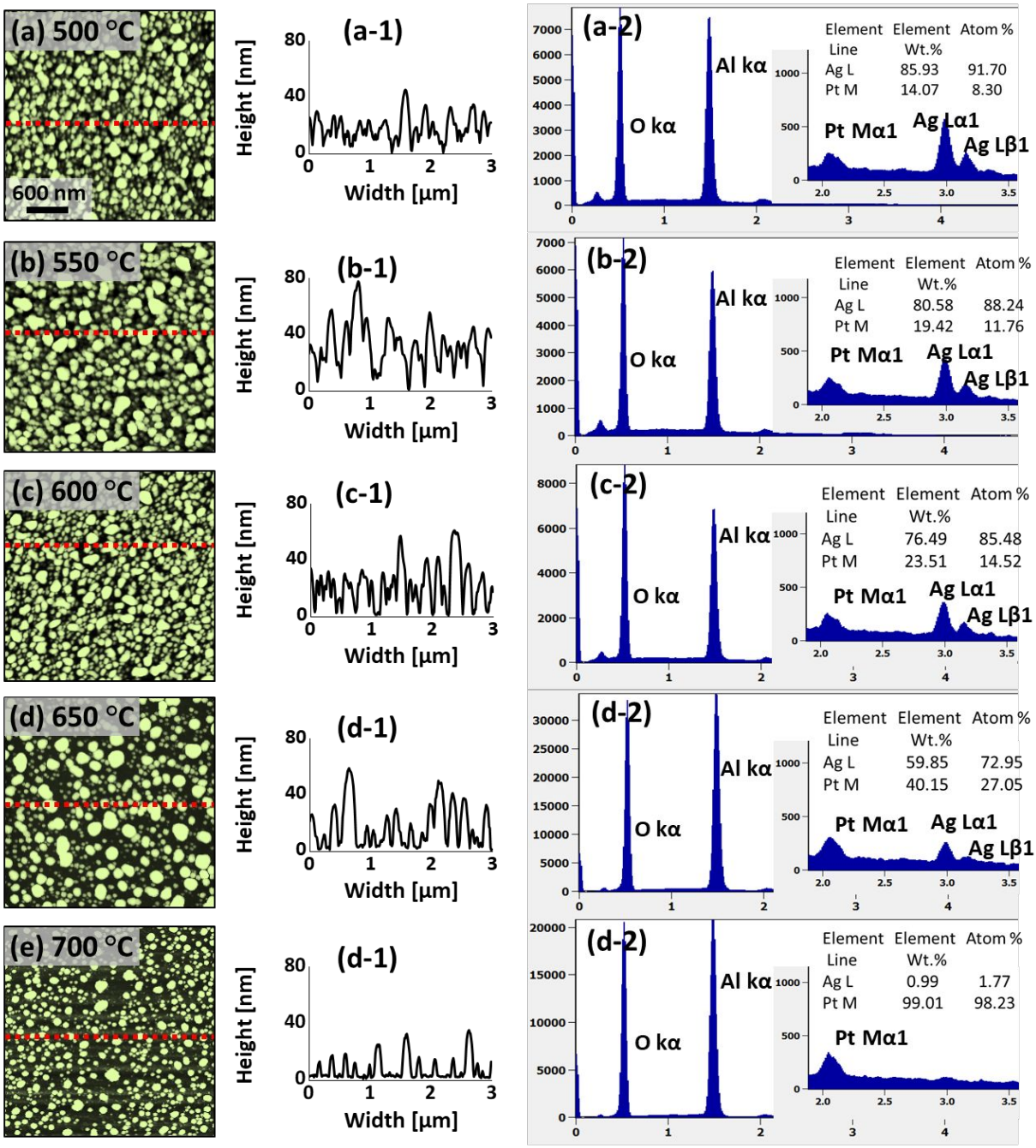

Figure S6: Fabrication of AgPt and Pt NPs with $Ag_{10.5nm}/Pt_{2.25nm}$ bilayer film by annealing between 750 and 700 °C. (a) – (d) AFM side-views of 3 × 3 µm^2. (a-1) – (de-1) Corresponding line profiles of AFM side-views. (a-2) – (d-2) EDS spectra of corresponding samples. Corresponding insets show the enlarged Pt and Ag peaks and elemental compositions in terms of at % and wt %.

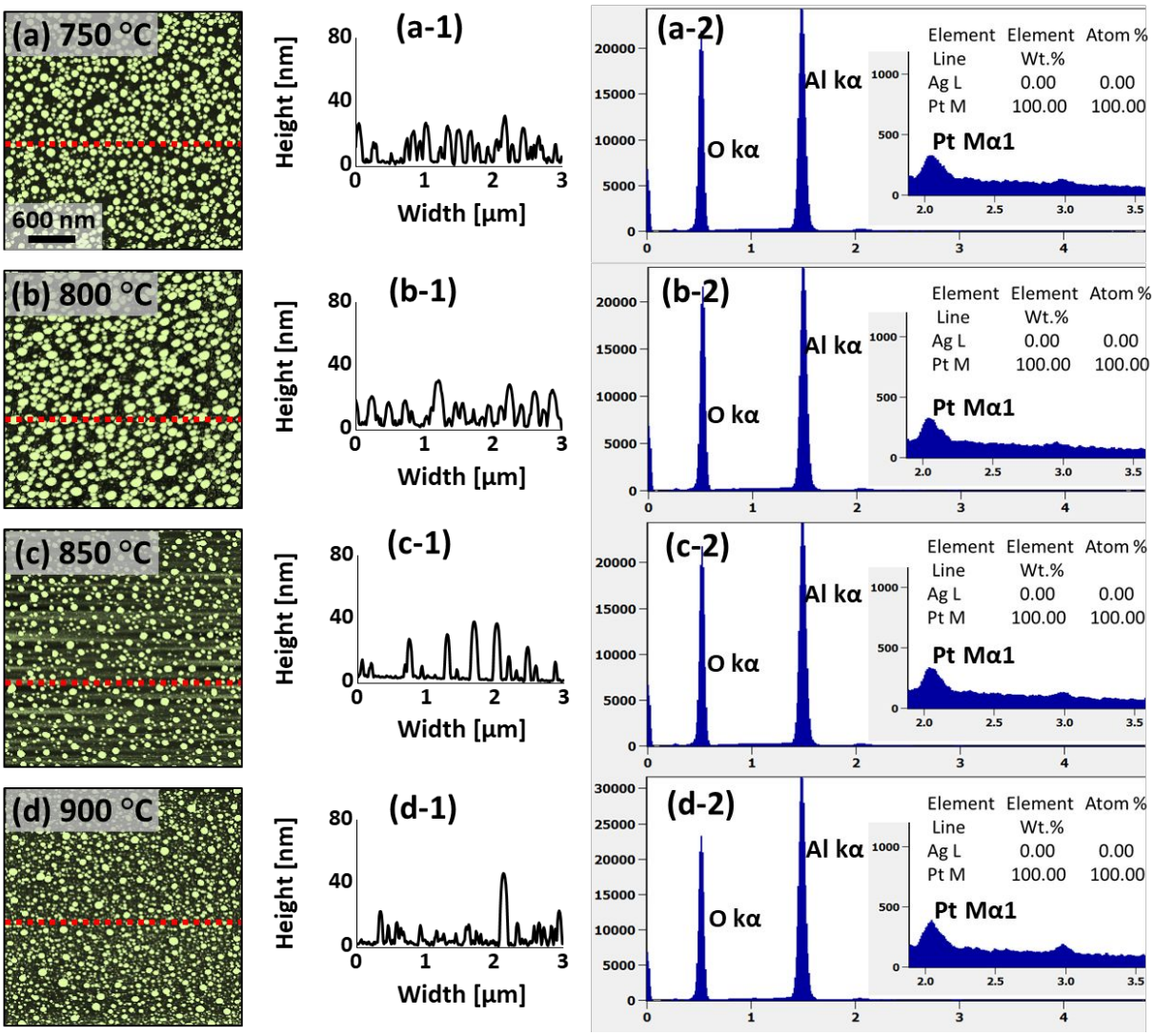

Figure S7: Evolution of Pt NPs between 750 and 900 °C with the $Ag_{10.5nm}/Pt_{2.25nm}$ bilayer film. (a) – (d) AFM side-views of 3 × 3 µm^2. (a-1) – (d-1) Corresponding line profiles of AFM side-views. (a-2) – (d-2) EDS spectra of corresponding samples. Corresponding insets show the enlarged Pt and Ag peaks and elemental compositions in terms of at % and wt %.

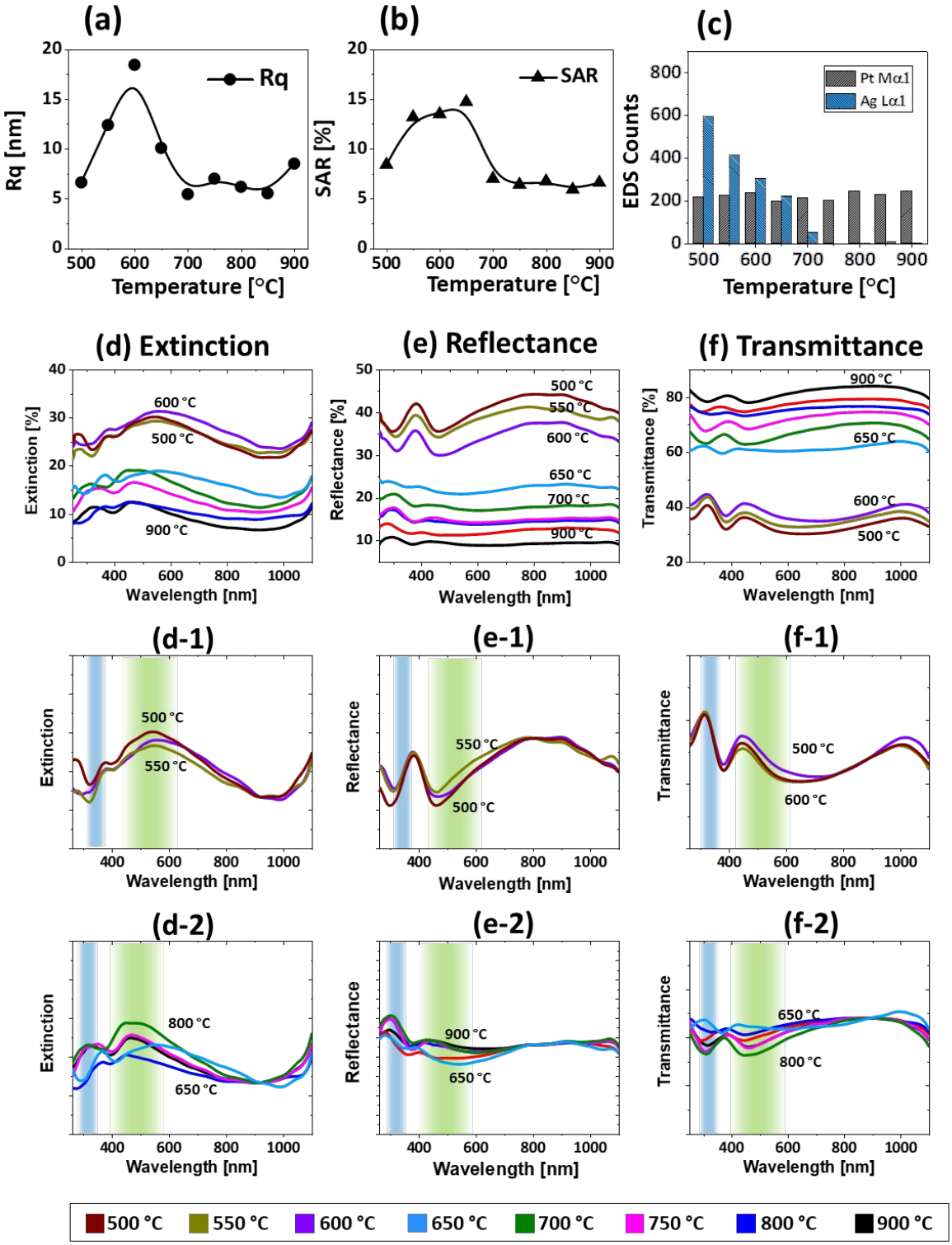

Figure S8: (a) – (c) Summary plots of the Rq, SAR and EDS count of the AgPt and Pt NPs fabricated with the $Ag_{10.5nm}/Pt_{2.25nm}$ bilayer films. (d) – (d-2) Extinction and normalized extinction spectra. (e) – (e2) Reflectance and normalized reflectance spectra. (f) – (f-2) Transmittance and normalized transmittance spectra.

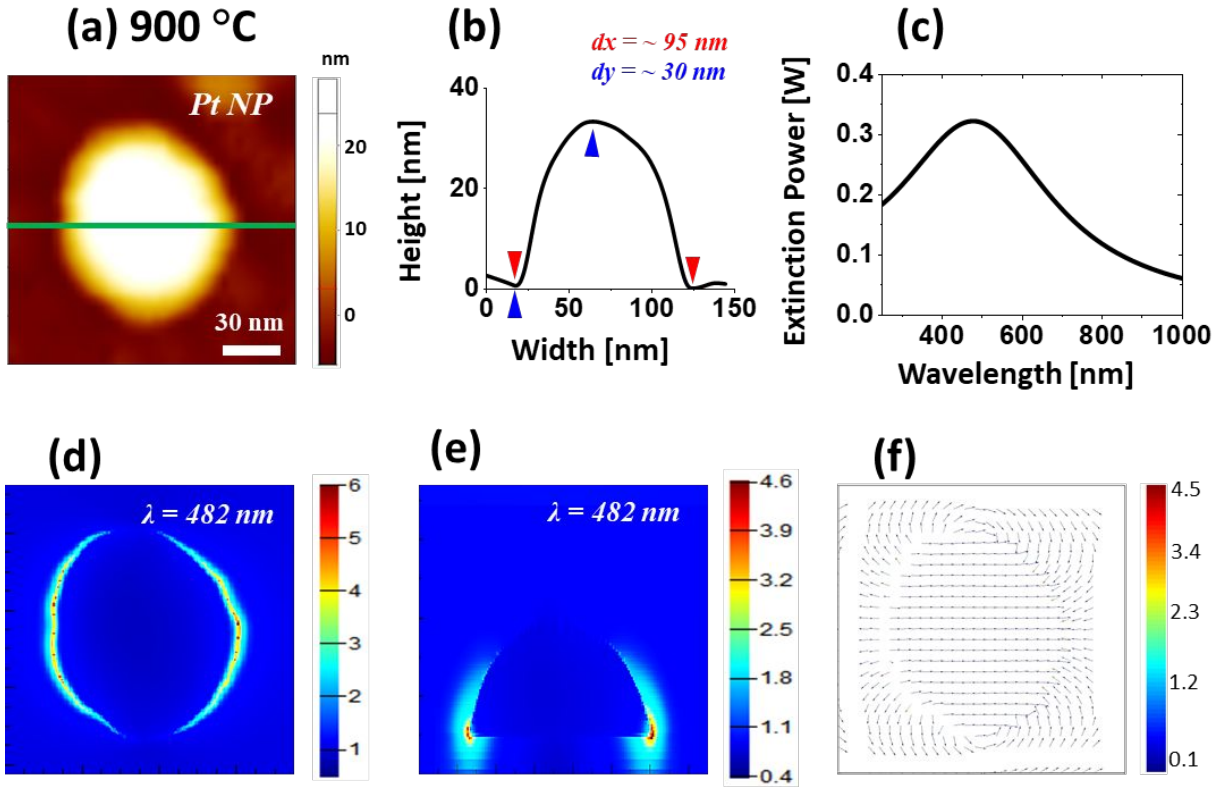

Figure S9: FDTD simulation of the Pt NP fabricated at 900 °C with the $Ag_{10.5nm}/Pt_{2.25nm}$ bilayers. (a) AFM image of the Pt NP. (b) Cross-sectional line profile. (c) Simulated extinction spectra. (d) – (e) E-field distribution in xy and xz plane at 482 nm. (f) E-field vector plot.

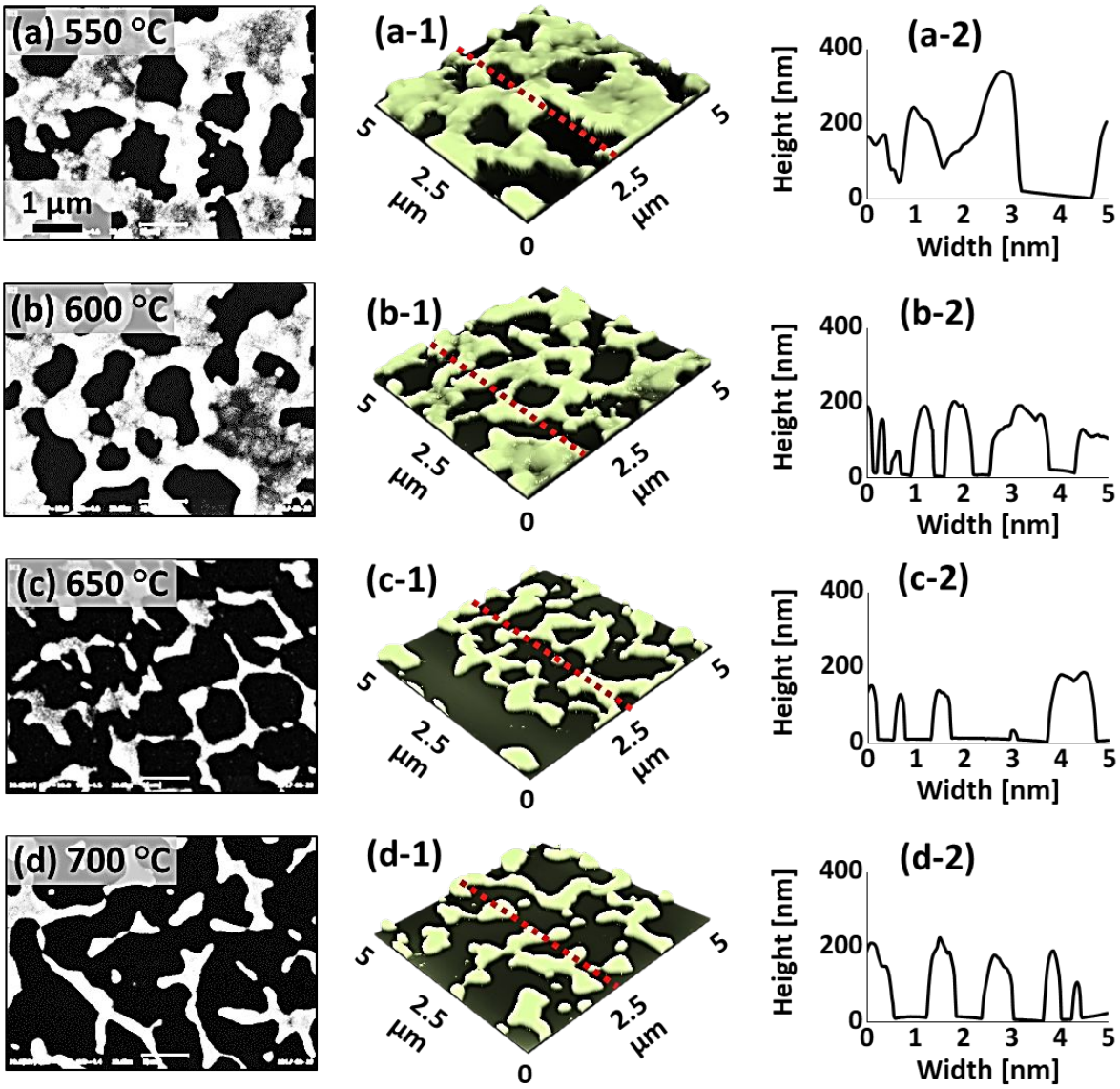

Figure S10: Large voids formation and alloy nanoclusters evolution from $Ag_{55nm}/Au_{15nm}/Pt_{15nm}$ tri-layers film by annealing between 750 and 900 °C for 120 s. (a) – (d) SEM images. (a-1) – (d-1) Corresponding AFM side-views. (a-2) – (d-2) Cross-sectional line profiles.

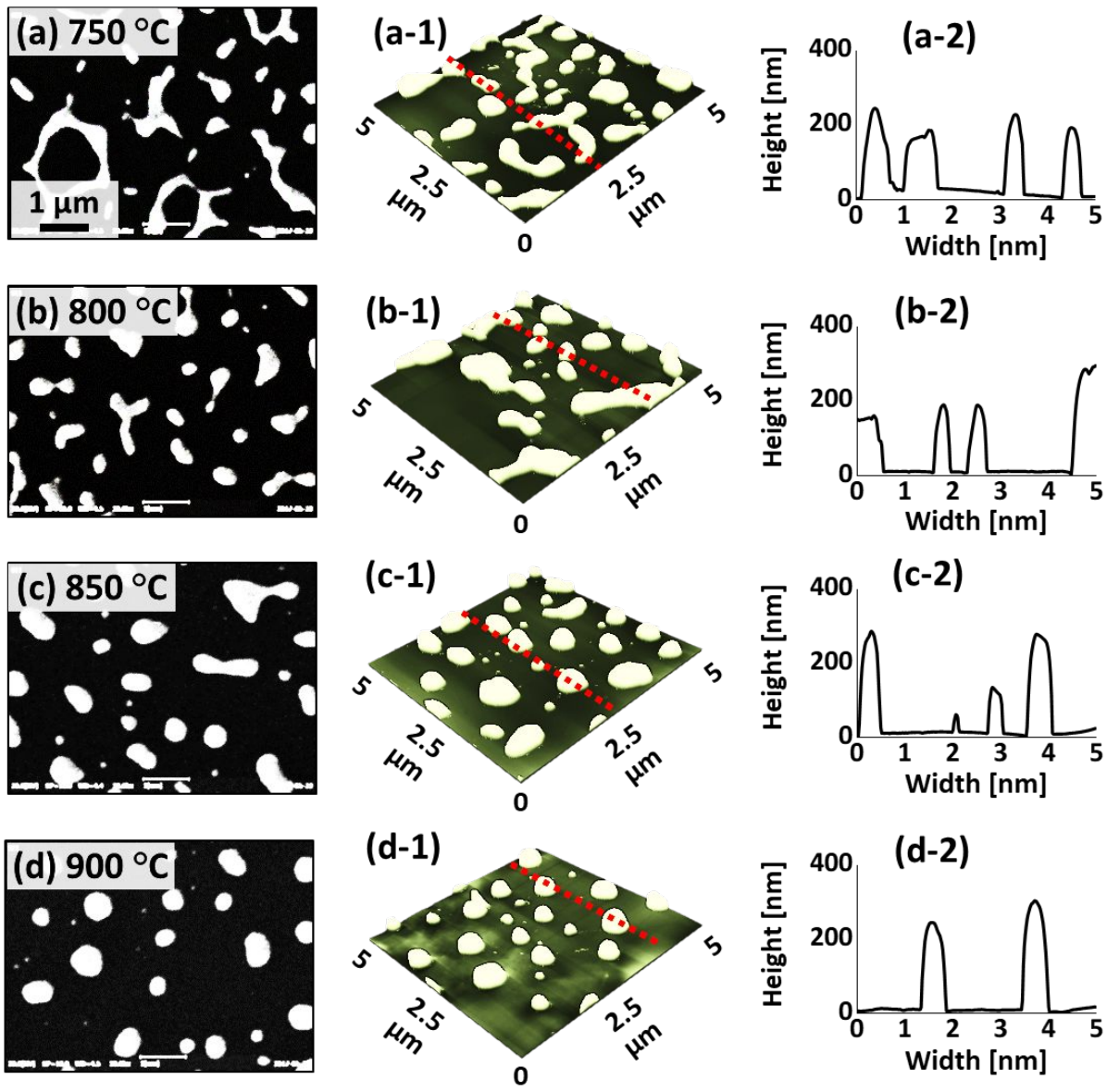

Figure S11: Evolution of voids and alloy nanoclusters from $Ag_{55nm}/Au_{15nm}/Pt_{15nm}$ tri-layers film by annealing between 750 and 900 °C. (a) – (d) SEM images. (a-1) – (d-1) Corresponding AFM side-views. (a-2) – (d-2) Cross-sectional line profiles.

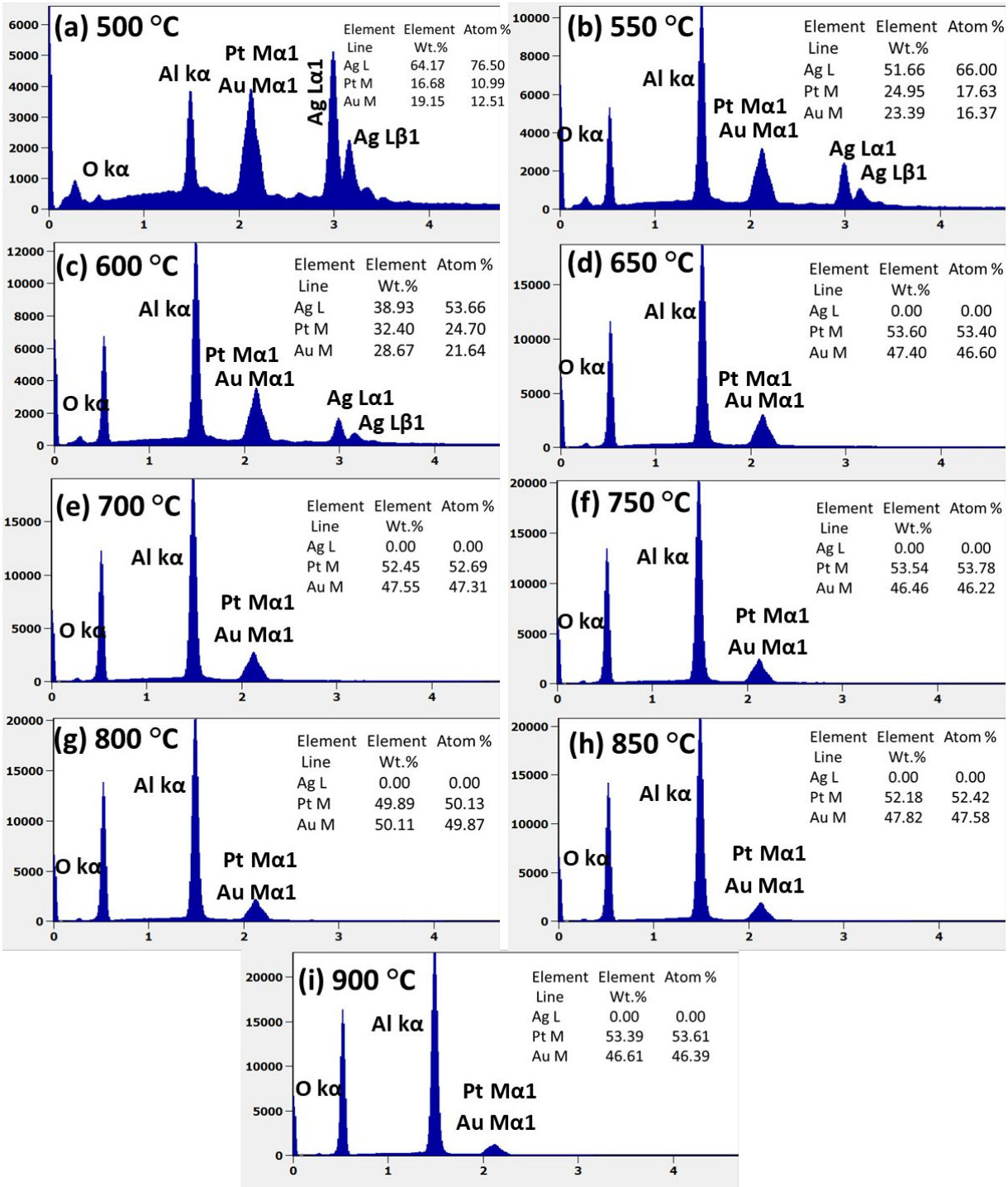

Figure S12: (a) – (i) EDS spectra of the samples fabricated with AgPt alloy NPs from $Ag_{55nm}/Au_{15nm}/Pt_{15nm}$ trilayers by annealing between 500 and 900 °C for 120 s. Corresponding insets show the enlarged Pt and Ag peaks and elemental compositions in terms of at % and wt %.

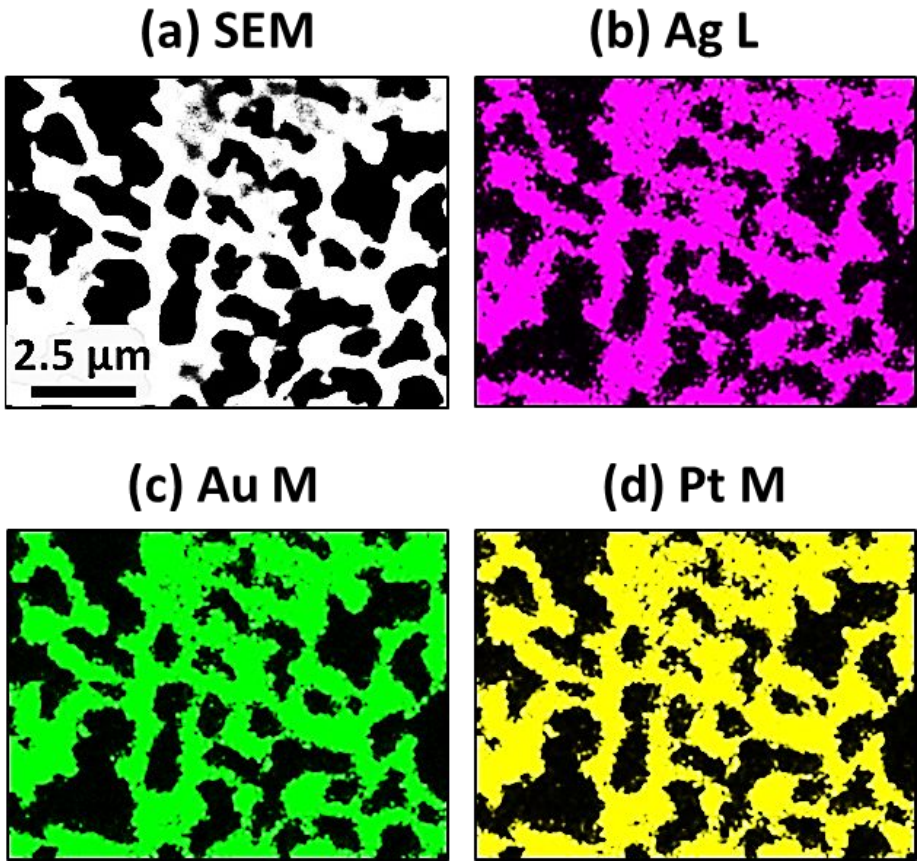

Figure S13: Elemental distribution analysis of the alloy nanostructure fabricated with $Ag_{55nm}/Au_{15nm}/Pt_{15nm}$ tri-layer at 600 °C. (a) - (d) SEM image and Elemental phases as labelled.

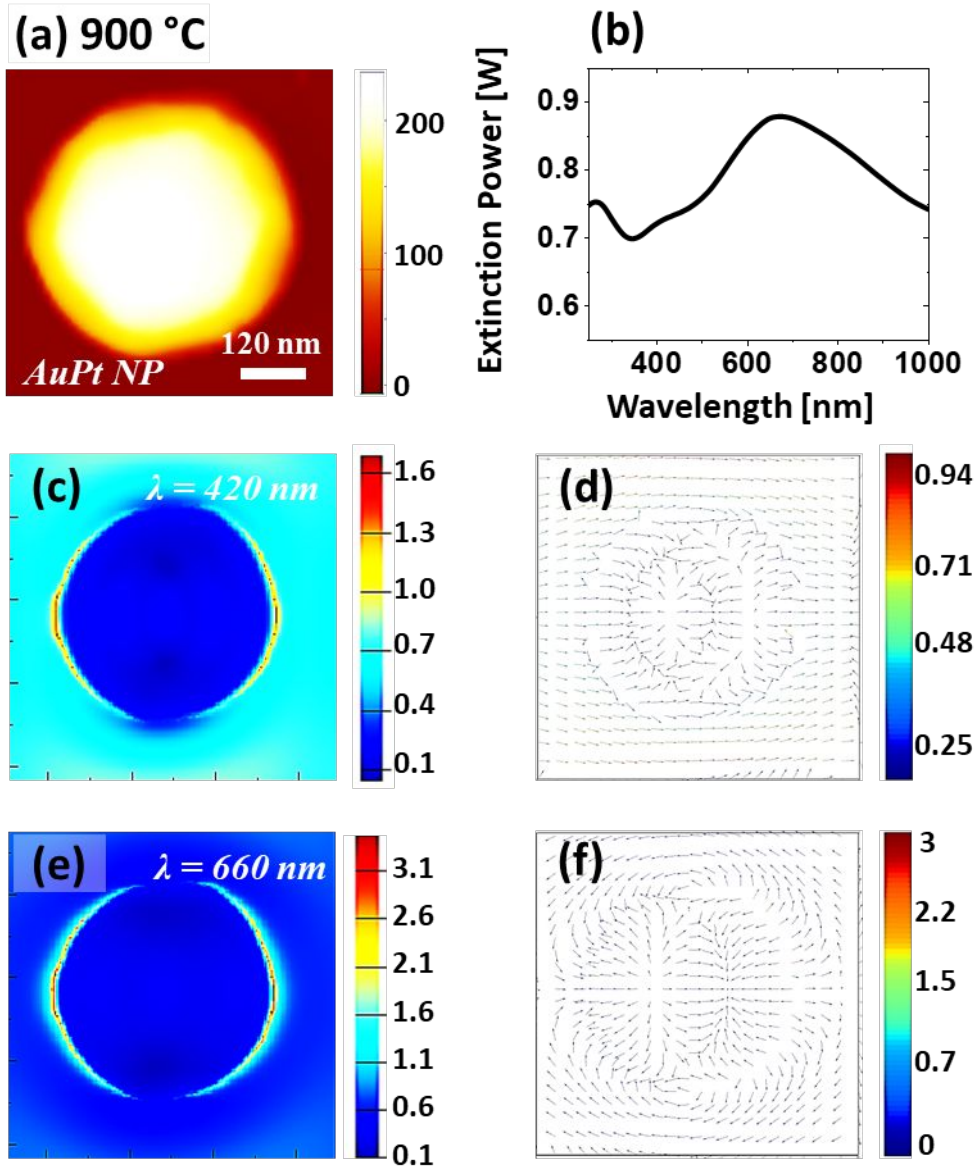

Figure S14: FDTD simulation of the medium size AuPt alloy NP fabricated with the $Ag_{55nm}/Au_{15nm}/Pt_{15nm}$ trilayers. (a) AFM image of typical NP. (b) Simulated extinction spectra. (c) – (d) E-field profile at 420 nm and corresponding e-field vector plot. (e)– (f) E-field profile and vector plot at 660 nm.

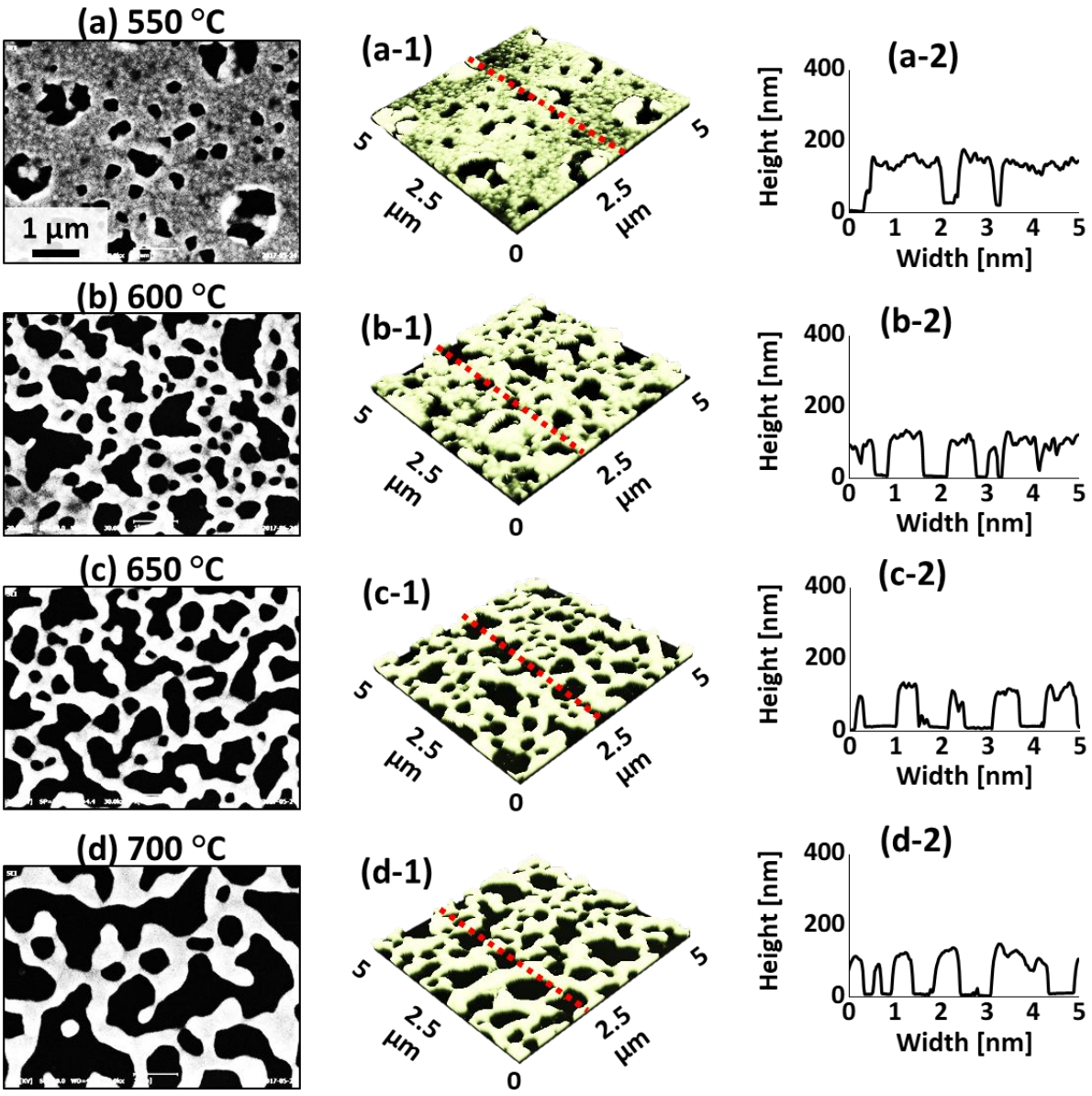

Figure S15: Evolution of large voids and alloy nanoclusters from $Ag_{40nm}/Au_{15nm}/Pd_{15nm}/Pt_{15nm}$ quad-layers by annealing between 750 and 900 °C. (a) – (d) SEM images. (a-1) – (d-1) Corresponding AFM side-views. (a-2) – (d-2) Cross-sectional line profiles.

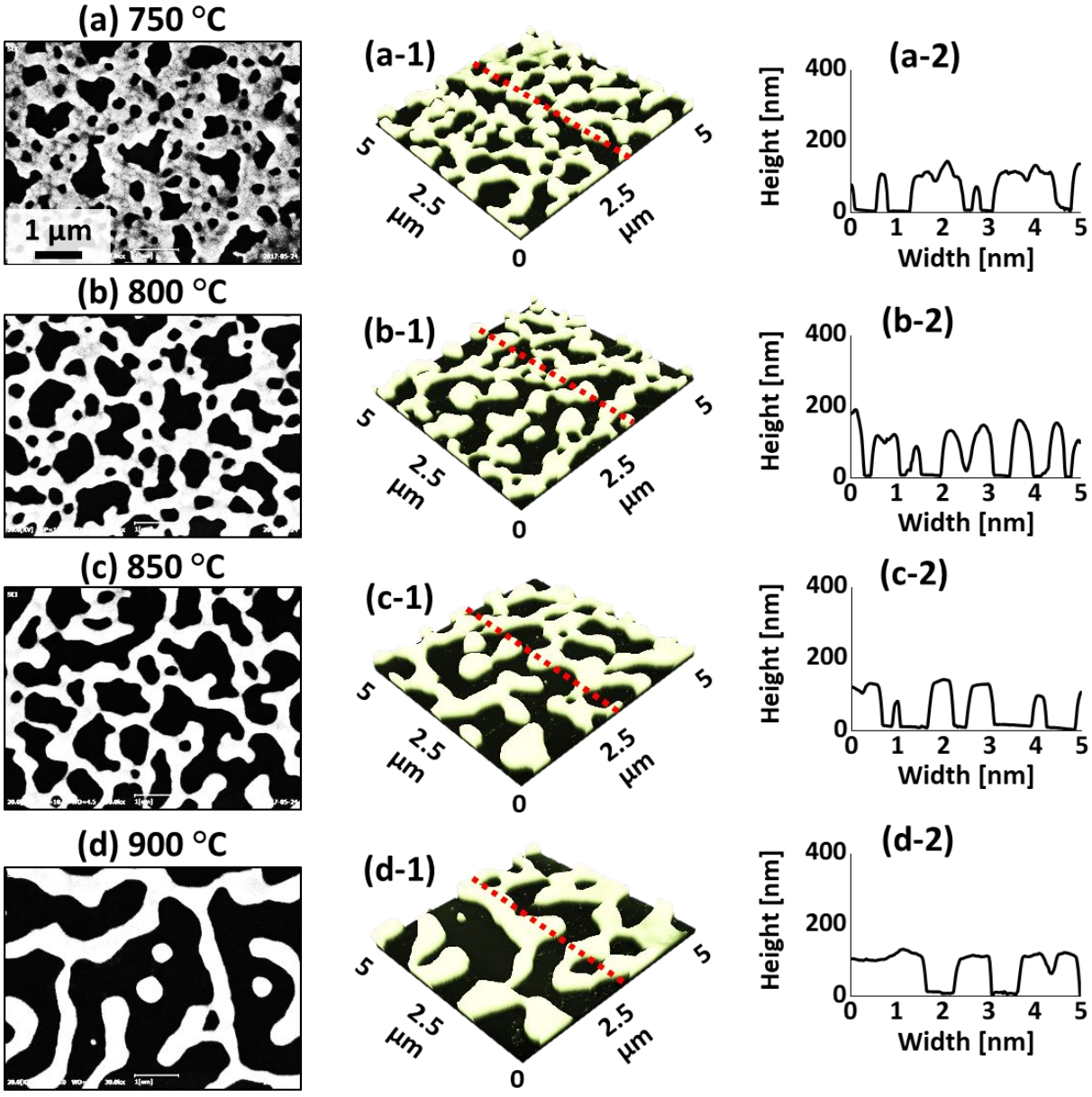

Figure S16: Evolution of connected nanoclusters from the $Ag_{40nm}/Au_{15nm}/Pd_{15nm}/Pt_{15nm}$ quad-layers film by annealing between 750 and 900 °C. (a) – (d) SEM images. (a-1) – (d-1) Corresponding AFM side-views. (a-2) – (d-2) Cross-sectional line profiles.

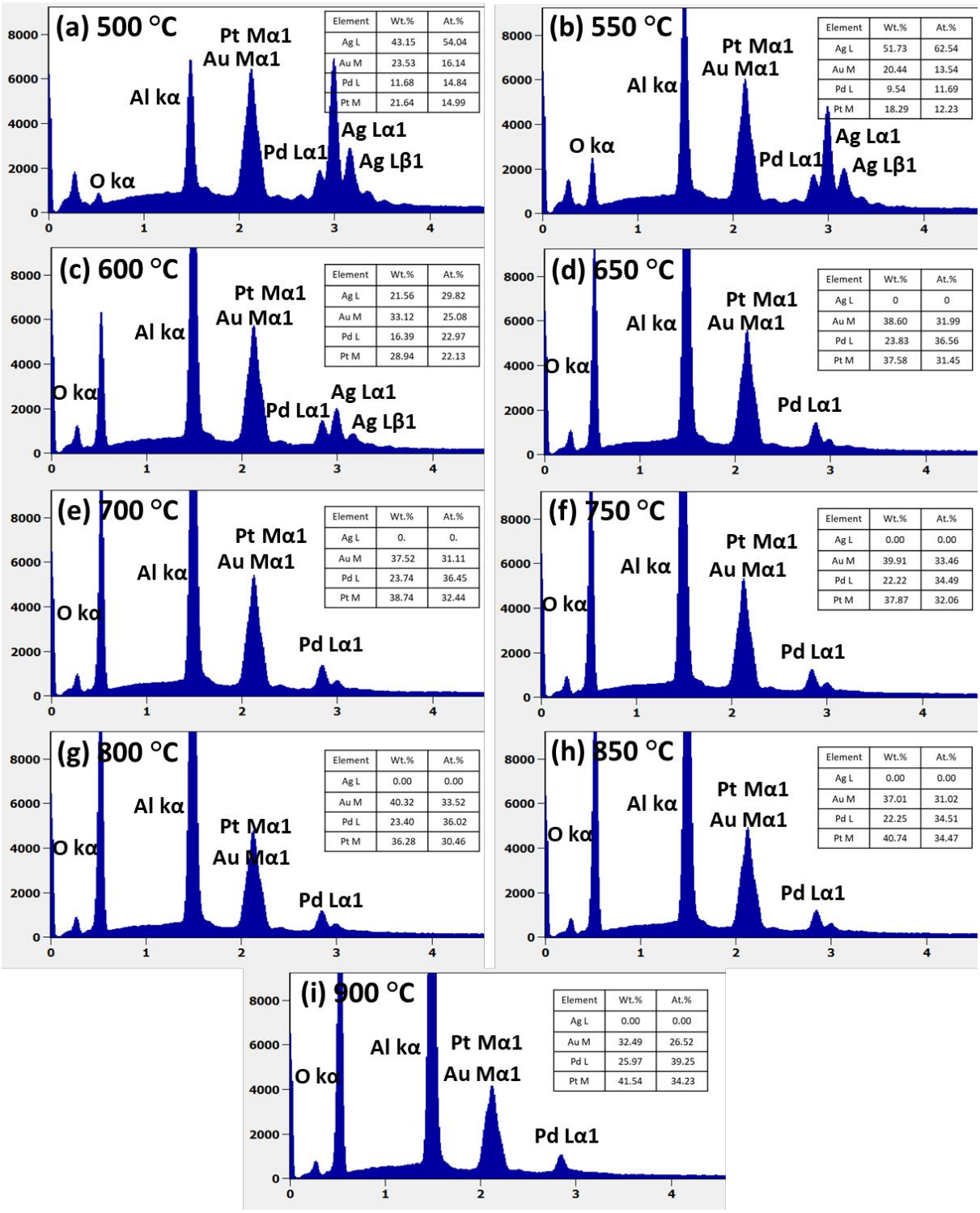

Figure S17: (a) – (i) EDS spectra of the samples fabricated with AgPt alloy NPs from $Ag_{40nm}/Au_{15nm}/Pd_{15nm}/Pt_{15nm}$ multilayer by annealing between 500 and 900 °C for 120 s. Corresponding insets show the enlarged Pt and Ag peaks and elemental compositions in terms of at % and wt %.

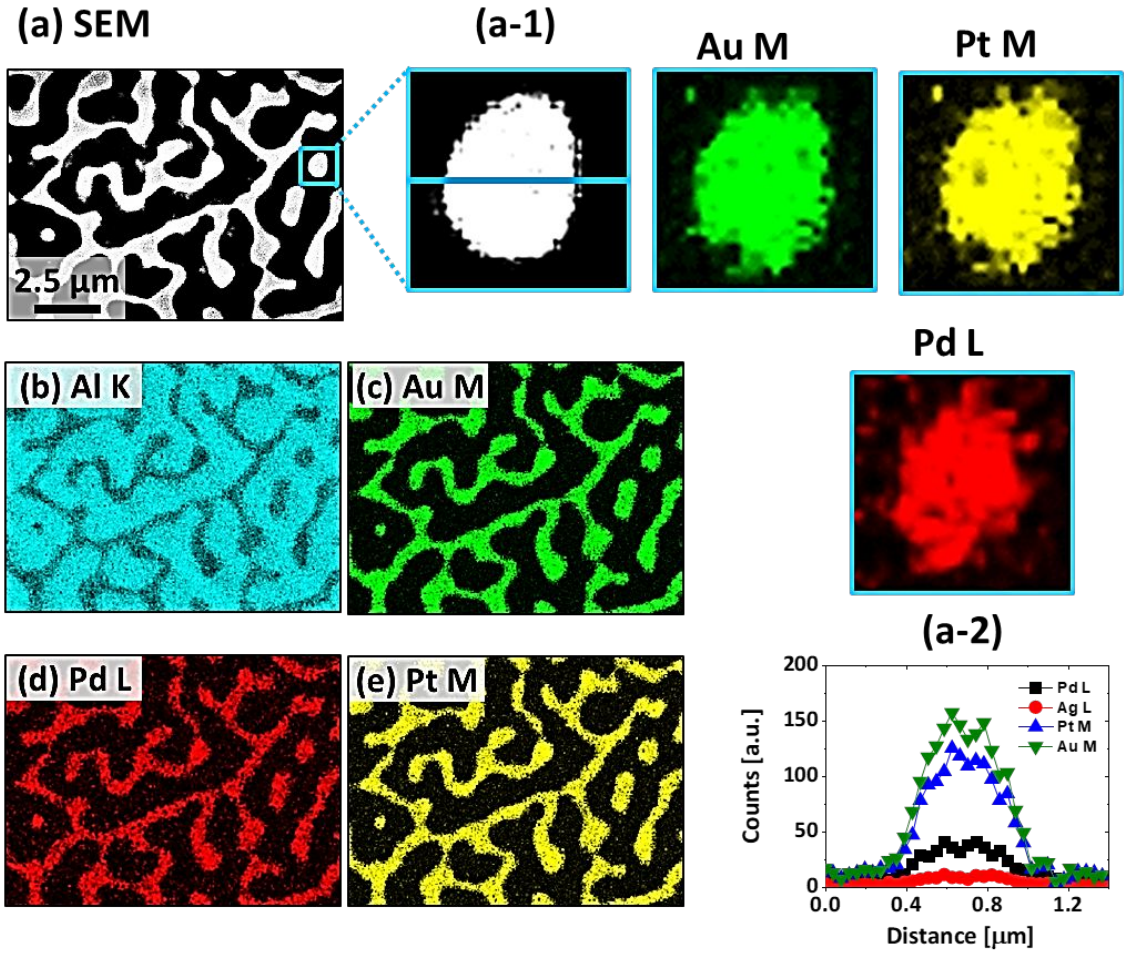

Figure S18: Elemental distribution analysis of alloy nanostructure fabricated with $Ag_{40nm}/Au_{15nm}/Pd_{15nm}/Pt_{15nm}$ multilayer composition. (a) – (e) SEM image and elemental phases as labelled. (a-1) – (a-2) Elemental phase map and line profile of the specific NP in (a).

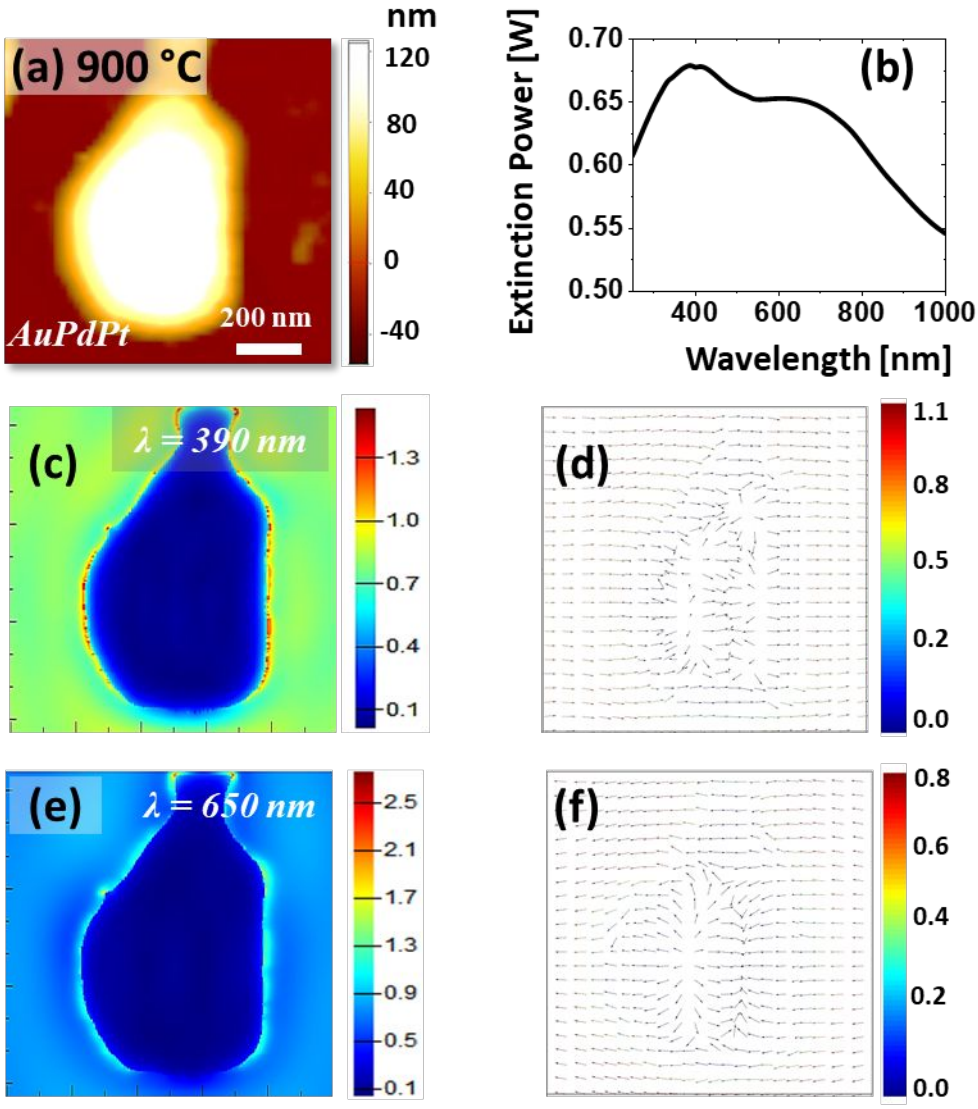

Figure S19: FDTD simulation of the typical AuPdPt alloy nanocluster fabricated with the $Ag_{40nm}/Au_{15nm}/Pd_{15nm}/Pt_{15nm}$ multilayer. (a) AFM image of typical NP. (b) Simulated extinction spectra. (c) – (d) E-field profile at 390 nm and corresponding e-field vector plot. (e)– (f) E-field profile and vector plot at 650 nm.